

# Critical thickness phenomenon in single-crystalline wires under torsion

Dabiao Liu<sup>1,2,3\*</sup>, Xu Zhang<sup>4</sup>, Yuan Li<sup>2</sup>, D. J. Dunstan<sup>2</sup>

<sup>1</sup>Department of Mechanics, Huazhong University of Science and Technology, Wuhan 430074, China

<sup>2</sup>School of Physics and Astronomy, Queen Mary University of London, London, E1 4NS, UK

<sup>3</sup>Hubei Key Laboratory of Engineering Structural Analysis and Safety Assessment, Wuhan 430074, China

<sup>4</sup>Applied Mechanics and Structure Safety Key Laboratory of Sichuan Province, School of Mechanics and Engineering, Southwest Jiaotong University, Chengdu 610031, China

\*Corresponding author: Dr. Dabiao Liu

E-mail: [dbliu@hust.edu.cn](mailto:dbliu@hust.edu.cn); or [dabiao.liu@qmul.ac.uk](mailto:dabiao.liu@qmul.ac.uk)

## Abstract

14 Analysis of idealised thin single-crystal wires under torsion based on the continuum theory of  
15 dislocations gives results in accordance with the critical thickness theory. The dislocation-free  
16 zone near the wire surface and the nearly-zero stress around the wire axis are predicted by  
17 both the continuum dislocation theory and critical thickness theory. It is demonstrated that  
18 the size effect at the onset of yielding, the distributions of stress and geometrically necessary  
19 dislocations in the thin wires in torsion, simply result from the critical thickness effect. A  
20 continuous increase of plastic strain from the neutral axis toward the wire surface is  
21 indicated. The plastic strain becomes (nearly) flat around the wire surface. Such a  
22 phenomenon is attributed to the fact that this is the region in which dislocations sources can  
23 operate, to provide the geometrically necessary dislocations required by the plastic strain  
24 gradient beneath. The results of continuum dislocation theory quantitatively elucidate the  
25 critical thickness phenomenon occurred in single-crystal wires under torsion. This links the  
26 continuum dislocation theory to the underlying physical picture of Matthews' critical  
27 thickness theory.

**Keywords:** Dislocations; Critical thickness; Size effects; Strain gradient plasticity; Torsion

## 1. Introduction

The size-dependent plasticity of micron-dimensioned metallic wires, i.e. the flow stress of metallic wires increasing with decreasing diameter, has attracted tremendous attention since the seminal work by Fleck *et al.* [1]. Torsion of thin metallic wires has been recognized as a benchmark experiment for exploring the strain-gradient effect at small scales [1-6] since it provides both the most sensitive and the most wide-ranging data in studies of the size effect in confined plasticity. In wire torsion, twist angle can be measured much more accurately than changes in length in tension or compression experiments [7, 8], or indentation depth in hardness testing [9]. Consequently, torsion experiments can readily span a range of strain from microstrain to more than unity, and have been crucial in revealing the size effect in soft metals in the yield strength and in the flow stress over at least six orders of magnitude in strain [1-3, 6, 10].

Conventional theories of plasticity are unable to predict the size-dependent phenomena since they do not involve any material length scales. Generally, the size effect associated to the non-uniform plastic deformation is attributed to the presence of geometrically necessary dislocations (GNDs [11, 12], sometimes they are called misfit dislocations [13], excess dislocations [14, 15], or non-redundant dislocations [16]). The size effect in the torsion of thin metal wires has been analyzed by using various theories, for examples, strain gradient plasticity (SGP) theories [1, 2, 17-27], stress gradient plasticity theory [28, 29], critical thickness theory (CTT) [3, 30, 31], continuum dislocation theory (CDT) [15, 16, 32, 33], and by molecular dynamics (MD) and discrete dislocation dynamics (DDD) simulations [34-40]. The dislocation configuration in a single-crystal thin wire undergoing torsion was firstly studied by Eshelby [41] in 1953 which is now referred to as the Eshelby twist. The author analyzed a screw dislocation lying along the axis of a thin rod (e.g. crystal whisker) which gives rise to the Eshelby twist. Gao *et al.* [17] considered a range of screw dislocations parallel with the wire axis as the admissible bundle of GNDs. Weertman and his co-workers [16, 42] and Duan *et al.* [43] concluded that the screw GNDs should lie in the planes orthogonal to the cylinder axis. Weertman [16] showed that it is impossible in plastically

1 isotropic metals for the anomalous hardening to result from twist boundaries formed by  
2 combining GNDs that are parallel to the wire axis and GNDs that are perpendicular to the  
3 wire axis because the sign of the GNDs in one set of dislocations of a cross-grid is opposite  
4 that of the other.

5 In conventional plasticity, for wire torsion, the onset of plasticity starts near the wire  
6 surface while no plasticity is developed in the center of wire. However, contradicting the  
7 classic plasticity, Dunstan and Bushby [30] predict a dislocation-free thickness near the  
8 surface of a wire under torsion according to Matthews' critical thickness theory [13]. Such a  
9 critical-thickness phenomenon has been further confirmed by latter MD and DDD  
10 simulations [36, 38, 44, 45], by theoretical analysis based on the continuum dislocation  
11 theory [15, 32, 46], and has also been observed in recent torsion experiment on  
12 bamboo-structured gold micron-scale wires [47]. Ziemann *et al.* [47] measured the evolution  
13 of plastic deformation along the radial direction within twisted bamboo-structure Au wires of  
14 diameter 25  $\mu\text{m}$ , using Laue microdiffraction. They found that the misorientation  
15 continuously increases from the wire axis toward the wire surface, and that the highest  
16 density of GNDs appears in the neutral center of wire. Therefore, the critical thickness effect  
17 happens for the defect-free single-crystal wire where dislocations can move freely inward the  
18 wire. Moreover, when a wire is under torsion, screw dislocations can escape from the wire  
19 surface if the surface is traction-free. So, there must be a dislocation-free zone near the wire  
20 surface for the wire to be at equilibrium.

21 Experimental data from wire torsion yields only torque-twist curves which do not  
22 necessarily discriminate adequately between different theories of the size effect [1-3]. It is  
23 valuable to be able to complement experimental data with the DDD or MD simulations and  
24 with the theoretical prediction based on CDT, which are capable of providing the distribution  
25 of dislocations in twisted wire. In particular, one can see directly how the GNDs required by a  
26 plastic strain gradient arrange themselves in the DDD simulation [34, 35] or in the analysis  
27 based on continuum dislocation theory [15, 16, 32, 33]. This information is crucial in deciding  
28 among the different theories of the size effect and in understanding plasticity in constrained  
29 volumes.

1 In a previous paper [44], we have shown that in the bending of thin foils the GNDs  
2 collected in the vicinity of the neutral plane, and accordingly this is the region in which there  
3 is a plastic strain gradient. Between this region and the free surfaces of the foil, the plastic  
4 strain is nearly constant so this region is GND-free. The elastic strain gradient here is close to  
5 the gradient of the applied (total) strain. Results were quantitatively in agreement with CTT  
6 [13, 48-52], according to which dislocation sources can only be operated in the GND-free  
7 region and the strain-thickness product (integral) in this region is a constant determined by  
8 the need to operate sources (for example, Frank-Read, spiral, or single-armed source) [30, 50,  
9 52]. In this work, we address the additional complexities of the dislocation distribution in  
10 thin crystal wires under torsion, and perform a comparison between the prediction of CTT  
11 and CDT.

12 The current paper is organized as follows. In Section 2, critical thickness theory is revisited.  
13 Key predictions for the problem of torsion of thin metal wires are given based on CTT. In  
14 Section 3, the framework of the continuum dislocation theory is summarized. In Section 4,  
15 the elasto-plastic torsion of the single-crystal wires under zero dissipation is analyzed based  
16 on the continuum dislocation theory. In Section 5, the main results for the problem of wire  
17 torsion given by the CTT and by the continuum dislocation theory are compared and  
18 discussed. Finally, conclusions are drawn in Section 6.

## 19 **2. Critical thickness phenomenon in wire under torsion**

### 20 **2.1 Physical picture of the critical thickness theory**

21 Matthews' critical thickness theory is based on the idea, firstly addressed by Frank and van  
22 der Merwe [53], that misfitting epitaxial layers would be elastically strained if the  
23 introduction of a dislocation that reduces the elastic misfit strain nevertheless increases the  
24 total energy. Since the energy of a strained layer is proportional to the layer thickness, while  
25 the energy of a dislocation varies with the logarithm of the thickness, a critical thickness can  
26 be determined above which plastic relaxation is expected [54]. The required dislocations are  
27 referred to as misfit dislocations or GNDs, since they are due to the misfit between the layer

1 and the substrate, and the introduction of these dislocations leads to a plastic strain gradient  
 2 or discontinuity for which the presence of the dislocations is necessary from geometrical  
 3 arguments. There are plenty of references on the calculation of critical thickness for epitaxial  
 4 layers [13, 48, 50-52, 54]. According to CTT, dislocation sources can only operate in the  
 5 GND-free region and the strain-thickness integral in this region is a constant. The Matthews'  
 6 critical thickness equation [30] gives

$$7 \quad h_c = \frac{Ab}{\varepsilon_0} \ln \frac{h_c}{Bb} \quad (1)$$

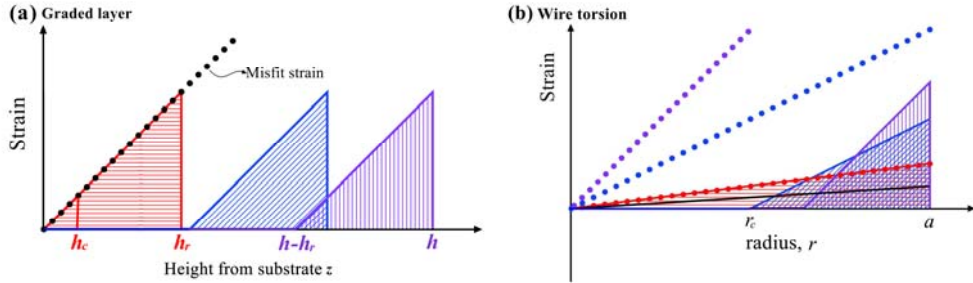
8 where  $A$  and  $B$  are two constants,  $\varepsilon_0$  the misfit strain,  $b$  the value of the Burgers  
 9 vector of the misfit dislocations. This equation predicts the critical thickness  $h_c$  at which  
 10 misfit dislocations (GNDs) may be generated by extending existing dislocations for relieving  
 11 the elastic strain in a simple layer with misfit strain  $\varepsilon_0$ . Experimentally and theoretically, Eq.  
 12 (1) is very close to  $h_c \varepsilon_0 = b$ . For a linearly graded strained epitaxial layer, it allows the  
 13 mismatch strain in the growth of structures advance linearly. That is  $\varepsilon_0(z) = \chi z$ , where  
 14  $\chi$  is the strain gradient along the growth direction  $z$ . The strain-thickness integral  
 15 (product) can be calculated by integrating  $\varepsilon_0(z)$  over the thickness. In significant  
 16 relaxation, the condition is determined by the need to operate dislocation sources [30, 50].  
 17 In this case, a relaxation critical thickness  $h_r$  is needed. For structures of InGaAs [55], it  
 18 requires the value of  $h_r$  to meet the condition  $h_r \varepsilon_0 \sim 5b$ . The factor of five is a reasonable  
 19 approximation for the Frank-Read sources [49]. For graded layers [55],

$$20 \quad \int_0^{h_r} \varepsilon(z) dz = \frac{1}{2} \chi h_r^2 \sim 5b \sim 0.8 \text{ nm}. \quad (2)$$

21 We now focus on the torsion of wires, which is analogous to the growth of the graded  
 22 layer that has been well studied by using CTT [44, 56]. For both cases, plastic strain gradients  
 23 are necessarily present. The solution to the graded-layer problem is illustrated in Fig. 1 (a).  
 24 We denote the thickness of the layer as  $h$  which is increased with the growth of the layer. If  
 25  $h \geq h_r$ , the material is completely relaxed plastically from  $h - h_r$  to the substrate, which

1 generates the plastic strain gradient  $\chi^p$ ; while the domain from  $h-h_r$  to the surface at  
2  $h$  has no GNDs. Above the thickness  $h-h_r$ , a depth  $h_r$  is entirely strained elastically,  
3 having the lattice constant at  $h-h_r$ . As growth of the graded layer advances, the added  
4 stress is relieved by the glide of dislocations, whereas at the top of the layer at  $h$  the  
5 elastically-strained thickness (i.e.  $h_r$ ) is changeless. The solution for the wire under torsion  
6 is illustrated in Fig. 1 (b). This is very similar to the thin foil under bending [44], and to the  
7 growth of graded layer mentioned above. The neutral axis plays the same role as the  
8 substrate, and from the neutral axis to the free surface the wire behaves in the same manner  
9 as a graded layer. The difference is only that, for the graded-layer problem, the plastic strain  
10 gradient remains constant and the thickness of layer rises during growth. While for the wire  
11 under torsion, the thickness (wire radius) is constant and the plastic strain gradient rises with  
12 torsion. However, for any given thickness and strain gradient, the solution (Eq.(2)) is still valid  
13 if the critical condition of Eq. (2), at which GNDs initiates, is satisfied. It is significant to realize  
14 that, for the graded-layer problem, plastic deformation continues from the surface down to  
15  $h-h_r$ , which leaves a plastic strain gradient in the range  $z \in (0, h-h_r)$ . For the wire  
16 under torsion, in the similar way, plastic deformation proceeds from the surface to the axis of  
17 the wire, but produces a plastic strain gradient simply in the range  $r \in (0, r_c)$ . Here,  $a-r_c$   
18 represents the critical thickness for plastic relaxation of wire torsion, and  $a$  is the radius of  
19 the wire. Yet,  $h_r$  is constant,  $r-r_c$  decreases with torsion. In the following, we test the  
20 prediction that at the surface of the wire under torsion there is a region depleted of GNDs;  
21 the onset of yielding and the strain distributions in elastic-plastic deformation agree with the  
22 idea.

23

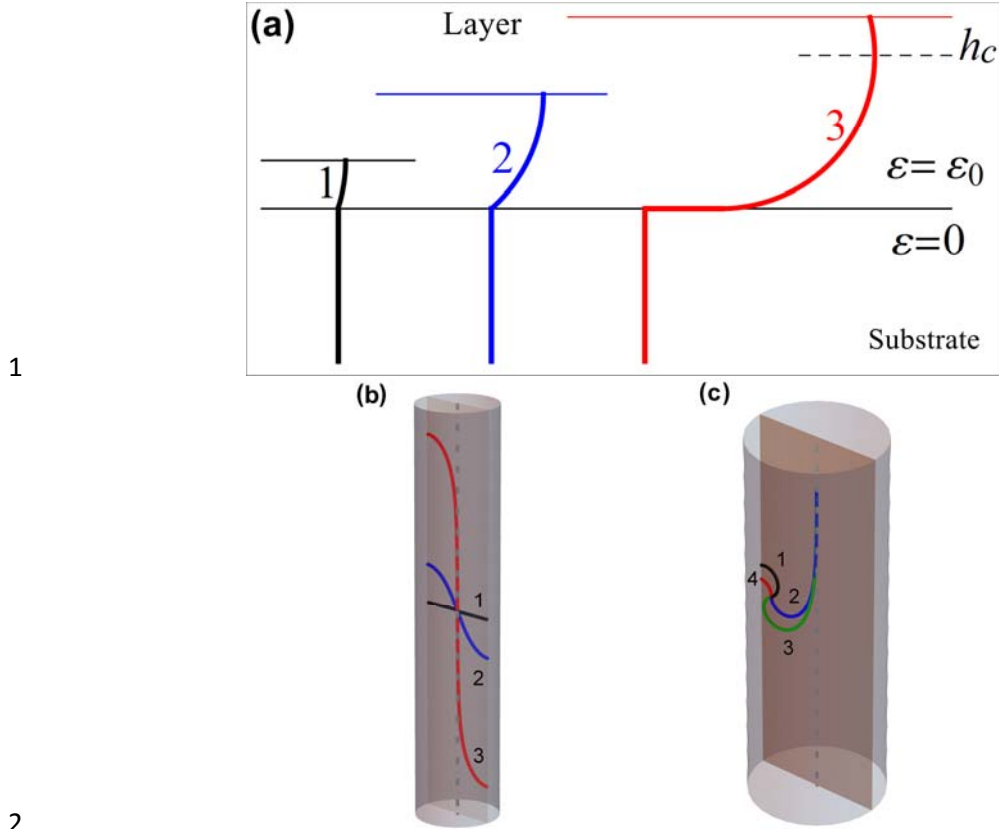


1

2 **Fig. 1.** Diagram of the critical thickness phenomenon for (a) the growth of graded layer and  
 3 (b) the wire under torsion. In (a), the misfit strain (the dotted line) is linear with height. For  
 4 thickness  $h \leq h_r$ , the elastic strain (thick solid line) is equal to the misfit strain, the dotted  
 5 line coincides with the thick solid line. When thickness  $h \geq h_r$ , the elastic strain from  
 6  $h - h_r$  to  $h$  (thick solid line) keeps the same slope as the dotted line and the triangular  
 7 area below it stays constant. In (b), the total strain is illustrated by the red dotted line going  
 8 through the origin. The area of the red triangle under the thick solid line (elastic strain) is the  
 9 constant strain-thickness integral. After more torsion, the total-strain line is the steeper  
 10 dotted blue line through the origin, and the elastic strain is the parallel solid blue line  
 11 delimiting steeper triangles of the same area as the red shaded triangle.

## 12 2.2 The Matthews' CTT applied to wire torsion

13 Now we apply Matthews' ideas directly to a thin crystal wire under torsion (see Fig. 2).  
 14 We firstly consider the Matthews CTT for epitaxial layers, as shown in Fig. 2(a). The  
 15 pre-existing dislocation (1) necessarily extends into the epitaxial layer as growth starts. As  
 16 growth continues, the dislocation curves sideways by the epitaxial strain (2). When the layer  
 17 thickness is above  $h_c$ , the dislocations lengthen indefinitely (3) creating a misfit dislocation.  
 18 In Fig. 2(b), a threading dislocation on a diameter of the wire follows the same evolution (1),  
 19 curving on a slip plane passing through the axis by torque (2). When the critical condition is  
 20 met, it prolongs indefinitely (3). Figure 2(c) shows the evolution of a well-placed spiral source  
 21 through the series of position 1-2-3-4. The critical condition for operation of the source is  
 22 that the stress is sufficient to swing the section 2 through 180° and the section 4 through 90°.



2  
3 **Fig. 2.** The Matthews mechanism for critical thickness is illustrated for epitaxial layers (a) and  
4 wires in torsion (b) (After Dunstan [49]). The initial state in both cases is labeled (1): A  
5 threading dislocation which necessarily extends into the epitaxial layer as growth starts (a) or  
6 an initial dislocation on a diameter of the wire at zero torque (b). As growth continues in (a)  
7 the dislocation curves under the layer stress (2), while in (b) the dislocation curves on a slip  
8 plane containing the axis (2) under the increasing torque. When the critical condition is  
9 exceeded, the dislocations extend indefinitely (3) creating a misfit dislocation in (a) and an  
10 axial dislocation giving Eshelby twist in (b). In (c) a well-placed spiral source is illustrated  
11 which evolves through the series of positions 1-2-3-4.

12 Following Matthews [13], one can determine the total elastic energy with and without the  
13 axial screw dislocation. As indicated by Dunstan *et al.* [3], the critical values of torsion angle  
14 or wire diameter can be calculated by equating these two energies. Let the axis be the  
15  $z$ -direction. The only nonvanishing component of the strain tensor is  $\varepsilon_{\theta z} = \kappa r$ , where  $\kappa$   
16 is the twist per unit length. The shear strain induced by the screw dislocation is  $b/(2\pi r)$

1 with  $b$  being the magnitude of the Burgers vector. We may subtract this from the torsion  
 2 strain field and symmetrise the strain tensor before integrating for the elastic energy. In  
 3 order to avoid the divergence as  $r \rightarrow 0$ , a core cutoff radius  $r_0$  as the lower integral limit  
 4 in the integrals is introduced. So, without the dislocation, the elastic energy of the wire per  
 5 unit length is

$$6 \quad \Psi_e = \frac{1}{2} \mu \int_{r_0}^a 2\pi r (\kappa r)^2 dr = \frac{1}{4} \pi \mu \kappa^2 (a^4 - r_0^4) \quad (3)$$

7 where  $\mu$  is the shear modulus,  $a$  is the radius of the wire. The energy with the  
 8 dislocation is

$$9 \quad \Psi_{ed} = \frac{1}{2} \mu \int_{r_0}^a 2\pi r \left( \kappa r - \frac{b}{2\pi r} \right)^2 dr = \frac{1}{4} \pi \mu \kappa^2 \left[ (a^4 - r_0^4) - \frac{2b(a^2 - r_0^2)}{\kappa \pi} + \frac{b^2 \ln(a/r_0)}{\pi^2 \kappa^2} \right] \quad (4)$$

10 Equating energies  $\Psi_e$  and  $\Psi_{ed}$ , we solve the critical value of  $\kappa$ ,

$$11 \quad \kappa_c = \frac{b}{2\pi(a^2 - r_0^2)} \ln \frac{a}{r_0} \approx \frac{b}{2\pi a^2} \ln \frac{a}{b} \quad (5)$$

12 Here,  $r_0 \sim b$  and  $a \gg b$  are used for giving the approximate expression. The core energy  
 13 of the dislocation, typically taken to be  $\frac{1}{2} \mu b^2$ , is usually accounted for by an additive (or  
 14 multiplying) factor within the logarithmic term. The formula Eq. (5) is useful because it  
 15 implies that the geometrical theory of critical thickness developed for flat surfaces [48] can  
 16 be used for curved surfaces as in wire under torsion.

17 The strain-thickness product or integral  $S$  is an important quantity in the Matthews  
 18 theory. If a misfit dislocation is terminated by a section rising to the free surface, it is the  
 19 value of  $S$  which determines the force on the termination. If this force is equal to the line  
 20 tension of the dislocation, the critical condition is satisfied. The force is independent of the  
 21 shape of the termination (roughly a quarter-circle for a simple epitaxial layer) and it is also  
 22 independent of the distribution of the strain within the thickness. Consequently,  $S$   
 23 provides a simple measure of the critical condition for more complicated problems [56] such  
 24 as, here, a strain rising linearly from the neutral axis to the surface. The critical value of  $S$   
 25 is

$$S_c = \int_0^a \kappa_c r \, dr \approx \frac{b}{4\pi} \ln \frac{a}{b} \quad (6)$$

2 Using the typical values  $a = 1\mu\text{m}$ ,  $b = 0.256\text{nm}$ ,  $r_0 = b$ , we obtain  $S_c \approx 0.17\text{nm}$ . This is  
 3 close to the approximate value for epitaxial layers [3, 48]. Correspondingly, the critical  
 4 stress-thickness product or integral is just  $S_c$  times the relevant elastic modulus. When the  
 5 critical torsion is achieved, the curvature of the dislocation is sufficient to take it through a  
 6 right angle between the axis and the surface of the wire, see the dislocation thread (3) of Fig.  
 7 2(b).

The strain-thickness product is also very useful for determining the critical condition for the operation of dislocation sources. All that is necessary is the topology of the source. The value of  $S_c$  is then multiplied by the number of quarter-circle equivalents that the source requires to fit into the space available, for example, five for a Frank-Read source or three for a spiral source in an epitaxial layer [50, 52, 57]. For the single-crystalline copper wire studied here, an optimally-placed source may thus require a  $S_c$  value of 0.45–0.75 nm, see Fig. 2 (c). Therefore, the radius beyond which the excess strain-thickness integral is about  $5b$ . So,

14 Therefore, the radius beyond which the excess strain-thickness integral is about 5b. So,

$$15 \quad S_c^* = \int_{r_c}^a \kappa r dr = \frac{1}{2} \kappa (a - r_c)^2 = 5b \Rightarrow r_c = a - \sqrt{\frac{10b}{\kappa}} \quad (7)$$

16 Then the ratio

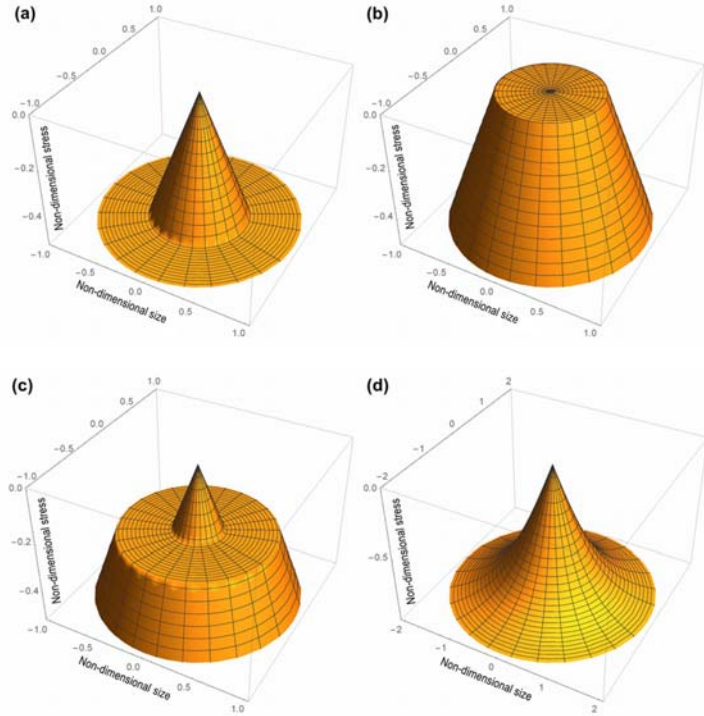
$$\xi = \frac{r_c}{a} = 1 - \sqrt{\frac{10b}{\gamma a}} \quad (8)$$

18 where  $\gamma = \kappa a$  is the surface shear strain. If  $r_c = 0$ , one can obtain the critical value of  $\kappa$   
 19 for the operation of dislocation sources. Taking  $a = 1 \mu\text{m}$ ,  $b = 0.256 \text{ nm}$ , we have  
 20  $\gamma_c = \kappa_c a = 0.00256$ . At the onset of yield, GNDs will first be situated at the radius  $r_c$ .  
 21 Under further torsion, these GNDs will be in a range from  $r_1$  to  $r_2$ , where  $r_1 < r_c < r_2$ .  
 22 With increasing torsion,  $r_2$  increases further, and the additional stress related to the region  
 23  $r_2 < r < a$  moves outward and enhances its contribution to the torque.

1 In Fig. 3, we compare the predictions of CTT for the form of the stress distributions with  
 2 the predictions of other plasticity theories. In the absence of any plasticity we take the stress  
 3 as proportional to  $r$ . Then in the absence of a size effect, for perfect plasticity  $\sigma(\varepsilon_p) = \sigma_0$ ,  
 4 we expect stress distributions of the form of Fig. 3(a). For critical thickness theory with no  
 5 bulk strength (size effect only), we expect the form of Fig. 3(b). If there is a bulk strength as  
 6 well as the size effect, we expect the form of Fig. 3(c) [30]. For the mechanistic  
 7 strain-gradient plasticity theory of Nix and Gao [28] we may write,

$$\begin{aligned}
 \varepsilon_p + \varepsilon_e &\propto r \\
 \rho_{\text{GND}} &\propto \partial_r \varepsilon_p \\
 \varepsilon_e &\propto \sqrt{\rho_{\text{GND}}}
 \end{aligned} \tag{9}$$

9 and solving for  $\varepsilon_e$  with the boundary condition  $\varepsilon_p|_{r=0} = 0$  we obtain  $\varepsilon_e \propto \tanh r$  as in  
 10 Fig. 3(d). One can see that the prediction of CTT (Fig. 3(c)) is a good approximation of the  
 11 prediction given by Nix-Gao model.



12  
 13 **Fig. 3.** The distribution of stress for a wire under torsion with some plastic deformation. (a)  
 14 perfect plasticity in continuum mechanics with a yield strength of  $\sigma_y = 0.5$ ; (b) critical

1 thickness theory with  $\sigma_y = 0$ ; (c) critical thickness theory with  $\sigma_y = 0.5$ ; and (d) the  
 2 strain-gradient theory of Eq. (9) with the constants of proportionality set to 1.

### 3 **3. Framework of continuum dislocation theory**

#### 4 **3.1 Dislocation density tensor in single crystal**

5 We consider a crystal with one slip system. The total strain of the crystal is the summation  
 6 of the elastic strain and the plastic strain. The plastic strain is

$$7 \quad \varepsilon_{ij}^P = \frac{1}{2}(\beta_{ij} + \beta_{ji}) \quad (10)$$

8 where  $\beta_{ij}$  is the plastic distortion. The elastic strain is obtained by subtracting the plastic  
 9 strain from the total strain,

$$10 \quad \varepsilon_{ij}^E = \varepsilon_{ij} - \varepsilon_{ij}^P = \frac{1}{2}(u_{i,j} + u_{j,i}) - \varepsilon_{ij}^P \quad (11)$$

11 where  $u_i$  is the displacement vector. For single slip system, the plastic distortion is  
 12 expressed by

$$13 \quad \beta_{ij} = \beta(\mathbf{x}) s_i m_j \quad (12)$$

14 where  $s_i$  is the slip direction vector,  $m_i$  the normal vector to the slip plane, and  $\beta(\mathbf{x})$   
 15 is an amount of slip on the corresponding active slip system. For the crystal with  $n$ -number of  
 16 slip systems, the plastic distortion can be expressed as  $\beta_{ij} = \sum_{\alpha=1}^n \beta^{(\alpha)}(\mathbf{x}) s_i^{(\alpha)} m_j^{(\alpha)}$  with  $\alpha$   
 17 denoting the slip systems. Generally, the continuous plastic distortion does not change the  
 18 volume, so we have  $\beta_{kk} = 0$ . It is obvious from Eq. (10) that the plastic distortion is exactly  
 19 the gradient of the plastic displacement field,

$$20 \quad \beta_{ij} = u_{i,j}^P \quad (13)$$

21 The plastic distortion tensor can also be written by

$$22 \quad \beta_{ij} = \varepsilon_{ij}^P + \omega_{ij}^P \quad (14)$$

1 where  $\varepsilon_{ij}^P$  and  $\omega_{ij}^P = \frac{1}{2}(\beta_{ij} - \beta_{ji})$  are the symmetric and antisymmetric parts of  $\beta_{ij}$ ,  
 2 respectively. Nye's dislocation-density tensor [11] is given by

3 
$$\alpha_{ij} = e_{jkl} \beta_{il,k} \quad (15)$$

4 where  $e_{jkl}$  is the (Levi-Civita) permutation symbol. We consider  $\alpha_{ij}$  as the fundamental  
 5 measure of the density of GNDs. For a crystal deforming in single slip, the density of GNDs  
 6 can be expressed as [58]

7 
$$\rho = \frac{|\alpha_{ij} n_j|}{b} = \frac{1}{b} |e_{jkl} \beta_{,k} m_l n_j|. \quad (16)$$

8 where  $n_j$  is the outward normal of the cut surface of the crystal, and  $b$  the magnitude of  
 9 Burgers vector.

## 10 3.2 Theoretical framework revisited

11 We analyze the torsion of thin single-crystalline wires by means of the continuum theory  
 12 of dislocation proposed by Berdichevsky [59, 60]. The main results of the continuum  
 13 dislocation theory are summarized here. In this theory, the free energy density is the sum of  
 14 the elastic energy density depending on the elastic strain tensor  $\varepsilon_{ij}^E$ , and the energy density  
 15 of microstructure depending on the dislocation density tensor  $\alpha_{ij}$ . It can be expressed as  
 16 [60, 61]

17 
$$\psi(\varepsilon_{ij}^E, \alpha_{ij}) = \frac{1}{2} \lambda (\varepsilon_{kk}^E)^2 + \mu \varepsilon_{ij}^E \varepsilon_{ij}^E + \psi_m(\alpha_{ij}) \quad (17)$$

18 where  $\lambda$  and  $\mu$  are the Lamé constants. The first two terms in Eq. (17) denote the  
 19 macroscopic elastic strain energy density of the crystal, and the term  $\psi_m(\alpha_{ij})$  represents  
 20 the energy of dislocation network [46, 60]. In the case of single crystal with single slip system,  
 21 this energy density can be expressed as

22 
$$\psi_m = \mu k \ln \frac{1}{1 - \rho/\rho_s} \quad (18)$$

1 where  $\rho$  is the scalar dislocation density,  $\rho_s$  the saturated dislocation density, and  $k$  a  
 2 material constant. As indicated by Berdichevsky [60], the logarithmic term guarantees that  
 3 the energy increases linearly for the small dislocation density  $\rho$ , and  $\psi_m \rightarrow \infty$  as  
 4  $\rho \rightarrow \rho_s$ . Therefore, this form of energy provides an energy barrier to avoid over-saturation.

5 For small density to moderate density of dislocations, the logarithmic term in Eq. (18) has  
 6 the following asymptotic formula

$$7 \quad \ln \frac{1}{1-\rho/\rho_s} \approx \frac{\rho}{\rho_s} + \frac{1}{2} \left( \frac{\rho}{\rho_s} \right)^2. \quad (19)$$

8 Alternatively, other forms of the defect energy have been proposed by Forest and  
 9 Guéninchault [62], Groma [63], Bardella and Panteghini [25].

10 Let  $\Omega$  be a domain occupied by the crystal in the initial state. The energy functional of  
 11 the crystal in the domain  $\Omega$  is

$$12 \quad E = \int_{\Omega} \psi(\varepsilon_{ij}^E, \rho) dV \quad (20)$$

13 where  $dV = dx_1 dx_2 dx_3$  represents the volume element. If energy dissipation is neglected,  
 14 the variational principle of the theory states that the true displacement field and the plastic  
 15 distortion in the final equilibrium state minimize the energy functional. That is

$$16 \quad \delta E = 0. \quad (21)$$

## 17 4. CDT applied to wire torsion

### 18 4.1 Energy functional

19 The problem of wire torsion has been studied by Kaluza and Le [32] based on CDT. We now  
 20 focus on the problem by comparing the results with those given by CTT. Consider a  
 21 single-crystalline wire of circular cross-section of diameter  $2a$  under monotonic torsion.  
 22 The wire is of length  $L$  and under twist  $\theta$  at its end. The Cartesian reference system  
 23  $(x_1, x_2, x_3)$  is set such that the  $x_1$  and  $x_2$  axes lie on the cross section of the wire, while

1 the  $x_3$  axis is the axis of the wire. A cylindrical coordinate system  $(r, \theta, z)$  is also  
 2 introduced for convenience, with  $z = x_3$ . We also assume that the active slip planes are  
 3 perpendicular to the vectors  $\mathbf{e}_\theta$  in the cylindrical coordinate system, while the slip  
 4 directions and the dislocation lines are parallel to the  $x_3$  axis. Actually, this assumption  
 5 cannot be met for any single crystal. However, since the Burgers' vector is parallel to a screw  
 6 dislocation, any crystallographic plane containing the dislocation is a possible slip plane [32].  
 7 For screw dislocations in the slip planes perpendicular to the vector  $\mathbf{e}_\theta$ , the only  
 8 nonvanishing component of plastic distortion is  $\beta_{z\theta} = \beta$ . Considering the symmetry of the  
 9 problem, we assume that  $\beta$  only depends on  $r$ . So, the non-zero components of the  
 10 plastic strain are

$$11 \quad \varepsilon_{\theta z}^P = \varepsilon_{z\theta}^P = \frac{1}{2} \beta(r) \quad (22)$$

12 Actually, for torsion of the rod here,  $\beta(r)$  equals to the plastic shear strain  $\gamma^P(r)$  since  
 13  $\varepsilon_{\theta z}^P = \varepsilon_{z\theta}^P = \frac{1}{2} \gamma^P(r)$ . The displacement field is

$$14 \quad u_\theta = \kappa z r, \quad u_r = u_z = 0 \quad (23)$$

15 Therefore, the non-vanishing components of the elastic strain tensor are

$$16 \quad \varepsilon_{\theta z}^E = \varepsilon_{z\theta}^E = \frac{1}{2} (u_{\theta,z} - \beta) = \frac{1}{2} (\kappa r - \beta) \quad (24)$$

17 From Eq. (15), the only non-vanishing component of Nye's tensor is

$$18 \quad \alpha_{zz} = \beta' + \beta/r \quad (25)$$

19 where  $(\bullet)' \doteq \frac{d(\bullet)}{dr}$ . Such a component of Nye's tensor is associated with the density of the  
 20 pure screw GNDs lying parallel to the axis of wire. From Eq. (16), the density of GNDs is

$$21 \quad \rho = \frac{1}{b} |\beta' + \beta/r|. \quad (26)$$

22 According to Eqs. (17), (19), (24), and (26), one can obtain the energy functional

1            $\psi(\beta) = 2\pi\mu \int_0^a \left[ \frac{1}{2}(\kappa r - \beta)^2 + \frac{k}{b\rho_s} \left| \beta' + \frac{\beta}{r} \right| + \frac{k}{2(b\rho_s)^2} \left( \beta' + \frac{\beta}{r} \right)^2 \right] r dr . \quad (27)$

2     This energy functional was firstly derived by Kaluza and Le[32]. In what follows, we study it  
3     further to give more results for comparing with the results obtained by CTT.

4     The density of GNDs must be a finite value at  $r=0$ , then, according to Eq. (26), we  
5     obtain the regularity condition

6            $\beta(0) = 0 \quad (28)$

7     which implies that the neutral axis of the wire should be seen as an obstacle hindering the  
8     motion of dislocations. So, the screw dislocations pile up around the neutral axis in  
9     equilibrium. This phenomenon is in agreement with the DDD simulation [64] and the  
10    prediction of CTT [3]. If we neglect the resistance to the dislocation glide, i.e. the dissipation  
11    is taken to be zero, the true plastic distortion (i.e. the plastic shear strain here) minimizes the  
12    energy functional (27) among all admissible function  $\beta(x)$  satisfying the regularity  
13    condition Eq. (28).

14    **4.2 The onset of yielding and the expression of torque**

15     For convenience, we introduce the following non-dimensional variables

16            $\bar{r} = \frac{r}{a}, \quad \gamma = \kappa a, \quad \eta = \frac{k}{ab\rho_s}, \quad F = \frac{\psi}{2\pi\mu a^2} \quad (29)$

17     Here, the variable  $\bar{r} \in [0,1]$ . The functional (27) is then reduced to be

18            $F(\beta(\bar{r})) = \int_0^1 \left[ \frac{1}{2}(\gamma\bar{r} - \beta)^2 + \eta \left| \beta' + \frac{\beta}{\bar{r}} \right| + \frac{\eta^2}{2k} \left( \beta' + \frac{\beta}{\bar{r}} \right)^2 \right] \bar{r} d\bar{r} \quad (30)$

19     We minimize the functional (30) among the function  $\beta(\bar{r})$  with the regularity condition  
20     $\beta(0) = 0$ . At  $\bar{r} = 1$ , it is traction-free and the dislocations can be annihilated, so there  
21    should be a dislocation-free zone near the free surface of the wire, as we discussed above.  
22    Therefore, the density of GNDs is zero, i.e.  $\beta' + \beta/\bar{r} = 0$ . This condition can be met if

1     $\beta = \beta_0/\bar{r}$ , where  $\beta_0$  is constant. This leads to the following assumption

$$2 \quad \beta(\bar{r}) = \begin{cases} \beta_1(\bar{r}) & \text{for } \bar{r} \in (0, \xi) \\ \beta_0/\bar{r} & \text{for } \bar{r} \in (\xi, 1) \end{cases} \quad (31)$$

3    where  $\xi$  is an unknown critical normalized radius,  $0 \leq \xi \leq 1$ , and  $\beta(\xi) = \beta_0/\xi$ . Next,  
4    we try to determine  $\beta_1(\bar{r})$  and the constants  $\beta_0$  and  $\xi$ . We assume  $\beta' + \beta/\bar{r} \geq 0$   
5    when  $\bar{r} \in (0, \xi)$  for the positive torsion  $\kappa$ . Then, the Eq. (30) becomes

$$6 \quad F = \int_0^\xi \left[ \frac{1}{2} (\gamma\bar{r} - \beta_1)^2 + \eta \left( \beta_1' + \frac{\beta_1}{\bar{r}} \right) + \frac{\eta^2}{2k} \left( \beta_1' + \frac{\beta_1}{\bar{r}} \right)^2 \right] \bar{r} d\bar{r} + \int_\xi^1 \frac{1}{2} (\gamma\bar{r} - \beta_0/\bar{r})^2 \bar{r} d\bar{r} \quad (32)$$

7    Varying the functional (32) with respect to  $\beta_1(\bar{r})$ , one can obtain the corresponding  
8    Euler-Lagrange equation in the range  $\bar{r} \in (0, \xi)$ , i.e.

$$9 \quad \beta_1'' + \frac{1}{\bar{r}} \beta_1' - \left( \frac{k}{\eta^2} + \frac{1}{\bar{r}^2} \right) \beta_1 = -\frac{k\bar{r}\gamma}{\eta^2} \quad (33)$$

10    The variation of Eq. (32) with respect to  $\xi$  and  $\beta_0$  gives two additional boundary  
11    conditions at  $\bar{r} = \xi$ , namely

$$12 \quad (\beta_1' + \beta_1/\bar{r}) \Big|_{\bar{r}=\xi} = 0 \quad (34)$$

13    and

$$14 \quad \sqrt{k} - \frac{1}{2} \frac{\sqrt{k}}{\eta} \gamma (1 - \xi^2) - \beta_0 \ln \xi = 0 \quad (35)$$

15    Eq. (33) is a non-homogeneous second-order modified Bessel differential equation. Its  
16    general solution can be obtained as [65]

$$17 \quad \beta_1(\bar{r}) = g(\bar{r}) + \left[ C_1 I_1 \left( \frac{\sqrt{k}}{\eta} \bar{r} \right) + C_2 K_1 \left( \frac{\sqrt{k}}{\eta} \bar{r} \right) \right] \quad (36)$$

18    where the expression in the square brackets is the general solution of the homogeneous  
19    modified Bessel differential equation,  $C_1$  and  $C_2$  are two constants to be determined by  
20    boundary conditions,  $I_n(\bullet)$  represents the modified Bessel function of the first kind of  
21    order  $n$ ,  $K_n(\bullet)$  denotes the modified Bessel function of the second kind of order  $n$ , and

1  $g(\bar{r})$  is a particular solution of Eq. (33). We can easily find a form of  $g(\bar{r})$ , e.g.

2       $g(\bar{r}) = \bar{r}\gamma$ . Since  $K_1\left(\frac{\sqrt{k}}{\eta}\bar{r}\right)$  is singular at  $\bar{r} = 0$ , the condition  $\beta_1(0) = 0$  implies

$$3 \quad C_2 = 0. So,$$

$$4 \quad \beta_1(\bar{r}) = \bar{r}\gamma + C_1 I_1\left(\frac{\sqrt{k}}{\eta} \bar{r}\right) \quad (37)$$

5 Using  $(\beta'_1 + \beta_1/\bar{r}) \Big|_{\bar{r}=\xi} = 0$ , we obtain

$$6 \quad C_1 = -\frac{2\gamma}{\frac{\sqrt{k}}{\eta} I_0\left(\frac{\sqrt{k}}{\eta}\xi\right)} \quad (38)$$

7 Since  $\beta_0 = \xi\beta_1(\xi)$ , we have

$$\beta_0 = \frac{I_2\left(\frac{\sqrt{k}}{\eta}\xi\right)}{I_0\left(\frac{\sqrt{k}}{\eta}\xi\right)}\xi^2\gamma \quad (39)$$

9 Substituting Eq. (39) into Eq. (35) leads to

$$10 \quad \sqrt{k} - \frac{1}{2} \frac{\sqrt{k}}{\eta} \gamma \left(1 - \xi^2\right) - \frac{I_2\left(\frac{\sqrt{k}}{\eta} \xi\right)}{I_0\left(\frac{\sqrt{k}}{\eta} \xi\right)} \xi^2 \gamma \ln \xi = 0 \quad (40)$$

11 This is a transcendental equation for determining  $\xi$  in terms of constants  $k$ ,  $\eta$  and  $\gamma$ .

12 The threshold value of surface shear strain,  $\gamma_{en}$ , is obtained when  $\beta_0 \rightarrow 0$ . For  $\gamma > \gamma_{en}$ ,

13 Eq. (40) has one root. Thus, substituting  $\beta_0 = 0$  into Eq. (40) and considering  $\xi \ll 1$  at  
 14 the onset of dislocation nucleation, we obtain

$$\gamma_{\text{en}} = \frac{2\eta}{1-\xi^2} \approx 2\eta \quad (41)$$

16 In terms of the original variables, we have

$$17 \quad \gamma_{\text{en}} = \frac{2k}{ab\rho_s} \Rightarrow K_{\text{en}} = \frac{2k}{a^2b\rho_s} \quad (42)$$

18 For  $\gamma \leq \gamma_{en}$  no dislocations are nucleated and the plastic distortion  $\beta = 0$ . Actually,  $\gamma_{en}$   
 19 is the surface shear strain at initial yielding. The value of  $\gamma_{en}$  is inversely proportional to the  
 20 wire radius, which shows an obvious size effect.

1 It is interesting to give the expression of torque for the torsion problem investigated here.

2 The torque can be derived by integrating the shear stress over the cross section of the wire,

3 
$$Q = 2\pi\mu \int_0^a (\kappa r - \beta(r)) r^2 dr = 2\pi\mu a^3 \int_0^1 (\gamma \bar{r} - \beta(\bar{r})) \bar{r}^2 d\bar{r} \quad (43)$$

4 For  $\gamma \leq \gamma_{en}$ , the plastic distortion  $\beta=0$ , so  $Q = \frac{1}{2}\pi\mu a^3 \gamma$ . For  $\gamma > \gamma_{en}$ , substituting Eq.

5 (31) into Eq. (43), we obtain

6 
$$Q = \frac{1}{2} a^3 \mu \pi \gamma \left[ \xi^4 \left[ 2 + \frac{k}{2\eta^2} (\xi^2 - 1) \right] \frac{{}_0\tilde{F}_1 \left( ;3; \frac{k\xi^2}{4\eta^2} \right)}{I_0 \left( \frac{\sqrt{k}}{\eta} \xi \right)} + (1 - \xi^4) \right] \quad (44)$$

7 where  ${}_0\tilde{F}_1$  denotes the regularized confluent hypergeometric function. Alternatively, Eq.

8 (44) may be derived by differentiating the strain energy  $\int_V \psi(\beta) dV$  with respect to  $\kappa$

9 since the torque  $Q$  is the work conjugate to  $\kappa$ . The torque can be rewritten in the

10 non-dimensional form  $\hat{Q}$ , i.e.

11 
$$\hat{Q} = \frac{Q}{\mu a^3} = \begin{cases} \frac{\pi\gamma}{2} & \text{for } \gamma \leq \gamma_{en} \\ \frac{\pi\gamma}{2} \left[ \xi^4 \left[ 2 + \frac{k}{2\eta^2} (\xi^2 - 1) \right] \frac{{}_0\tilde{F}_1 \left( ;3; \frac{k\xi^2}{4\eta^2} \right)}{I_0 \left( \frac{\sqrt{k}}{\eta} \xi \right)} + (1 - \xi^4) \right] & \text{for } \gamma > \gamma_{en} \end{cases} \quad (45)$$

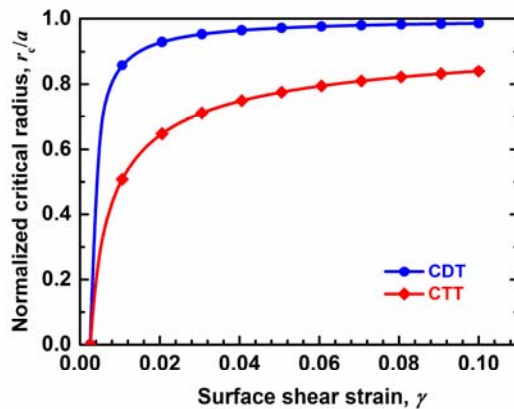
12 Evidently, the magnitude of  $\hat{Q}$  depends on the value of  $\gamma_{en}$ . The value of  $\gamma_{en}$  is  
 13 inversely proportional to the wire radius, which suggests that the non-dimensional torque  
 14 increases with decreasing the wire radius.

## 15 5. Results and discussions

16 In order to perform the calculation, we take the following parameters:  $b = 0.256\text{nm}$ ,  
 17  $k = 10^{-4}$ ,  $\rho_s = 3.05 \times 10^{14} \text{m}^{-2}$ , and  $a = 1\mu\text{m}$ . Note that the values of  $k$  and  $\rho_s$  are  
 18 assumed by equating  $\kappa_{en}$  in CDT (Eq. (42)) to  $\kappa_c$  in CTT (Eq. (7)). From Eqs. (29)<sub>3</sub> and (42),  
 19 we have  $\eta = 0.00128$ ,  $\gamma_c = \gamma_{en} \approx 0.00256$ .

## 1    5.1 The prediction of critical thickness

2    The trends of the critical radius  $\xi$  ( $= r_c/a$ ) with increasing the surface shear strain  
 3    predicted by CTT and CDT are compared in Fig. 4. In both theories, if  $\gamma \leq \gamma_{en}$ , the critical  
 4    radius is zero. After that, the critical radius increases as the surface shear strain increases.  
 5    Accordingly, the dislocation-free zone decreases with increasing the surface shear strain. If  
 6    we take values of  $k$  and  $\rho_s$  by assuming  $\gamma_{en} = \gamma_c$ , the critical radius given by CDT  
 7    increases with the surface shear strain more quickly than that of CTT, as shown in Fig. 4.



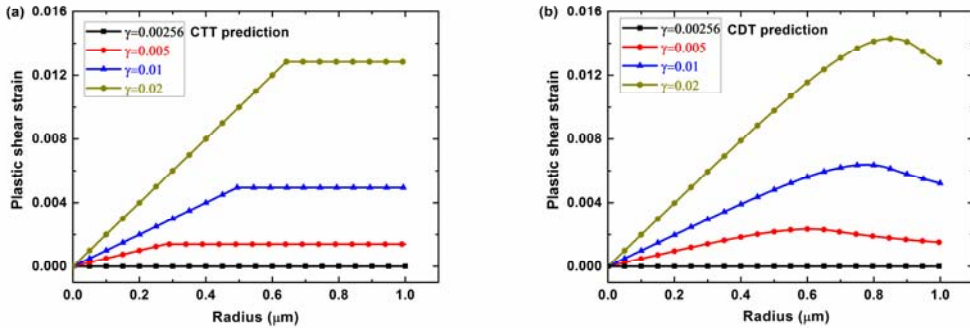
8  
 9    **Fig. 4.** The ratio of  $\xi = r_c/a$  as a function of surface shear strain  $\gamma$  in CTT and in CDT. The  
 10   lower curve is based on Eq. (8); the upper curve is based on Eq. (40).

11   The critical radii predicted by CTT (Eq. (8)) and CDT (Eq. (40)) at four values of surface  
 12   shear strain,  $\gamma = 0.00256, 0.005, 0.01$  and  $0.02$ , are given in Table 1. At a prescribed value of  
 13    $\gamma$ , the critical radius predicted by CDT is larger than that given by CTT. However, the  
 14   difference can be reduced by choosing another values of  $k$  and  $\rho_s$ .

15   **Table 1.** Normalized critical radius  $\xi$  predicted by CDT and CTT at different values of surface  
 16   shear strain.

Surface shear strain $\gamma$	0.00256	0.005	0.01	0.02
Critical radius by CTT ( $\mu\text{m}$ )	0	0.28	0.49	0.64
Critical radius by CDT ( $\mu\text{m}$ )	0	0.68	0.85	0.93

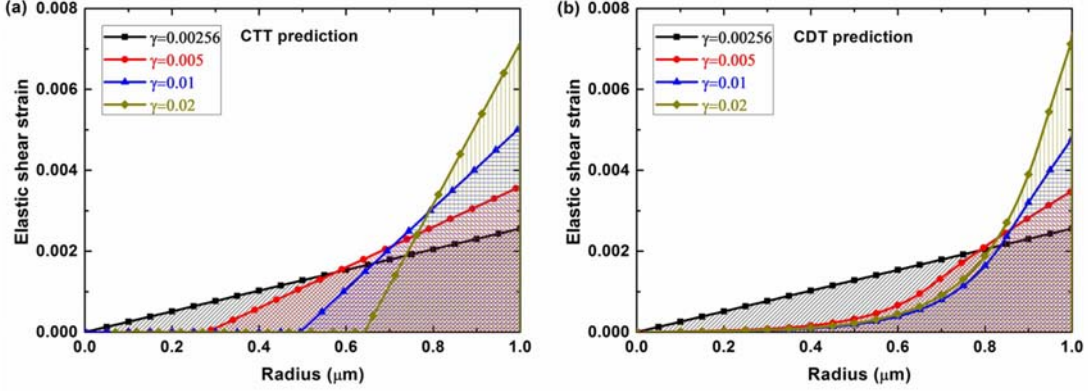
1  
 2     The distribution of the plastic shear strain along the wire radius predicted by CTT and CDT  
 3     are shown in Fig. 5. Below the threshold value of surface shear strain  $\gamma_{\text{en}} = \gamma_c \approx 0.00256$ ,  
 4     the plastic shear strain along the wire radius is zero. With the further increase of the surface  
 5     shear strain, the critical radius increases. In the range  $r \in (0, r_c)$ , for CTT, the plastic shear  
 6     strain increases linearly with the wire radius; while for CDT, the plastic shear strain increases  
 7     linearly with the wire radius at the beginning, and then tends to a plateau around  $r = r_c$ . In  
 8     the range  $r \in (r_c, a)$ , for the CTT, the plastic shear strain keeps a constant; while for CDT,  
 9     the plastic shear strain decreases with the wire radius.



10  
 11     **Fig. 5.** The distribution of plastic shear strain along the wire radius at different values of  
 12     surface shear strain. (a) Prediction by critical thickness theory; (b) Prediction by continuum  
 13     dislocation theory.

14  
 15     The distributions of the elastic shear strain  $\gamma^E$  across the radius of the wire at different  
 16     torsion are plotted in Fig. 6. When  $\gamma > \gamma_{\text{en}}$ , it is seen that the elastic shear strain nearly  
 17     vanishes at  $\bar{r} \in (0, \xi)$ . Accordingly, the shear stress is also nearly-zero in this range, i.e.  
 18     around the neutral axis of the wire. The strain-thickness product in CTT, the area of the  
 19     shaded part below the solid line, is a constant about  $0.00128 \mu\text{m}$ , while the strain-thickness  
 20     product in CDT changes from  $0.00128 \mu\text{m}$  to  $0.00109 \mu\text{m}$  with increasing torsion from  
 21      $\gamma=0.00256$  to  $0.02$ . Yet, the predictions given by CCT and CDT are in qualitative agreement

1 with each other.



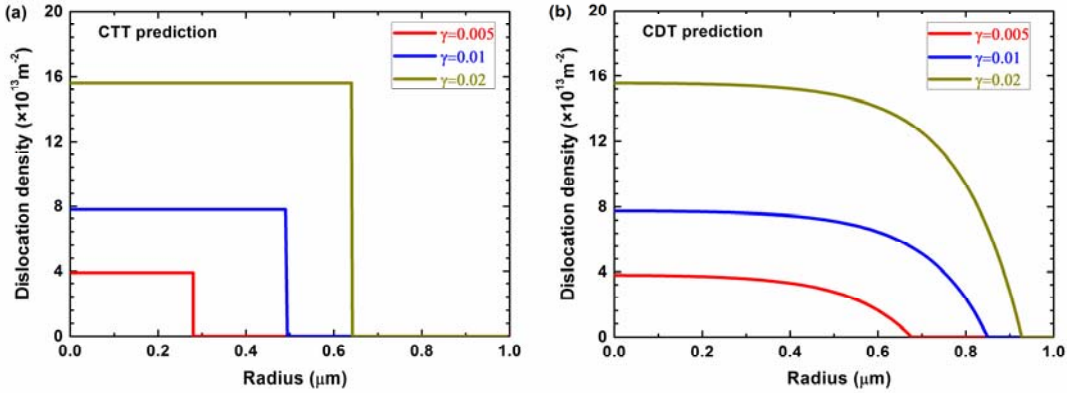
2  
3 **Fig. 6.** The distribution of the elastic strain with the radius of wire at different surface shear  
4 strain: (a) Prediction by CCT, the predicted strain-thickness is  $0.00128\mu\text{m}$ ; (b) Prediction by  
5 CDT, the predicted strain-thickness is  $0.00128$ ,  $0.000925$ ,  $0.000866$  and  $0.00109\mu\text{m}$  for  
6  $\gamma=0.00256$ ,  $0.005$ ,  $0.01$  and  $0.02$ .  
7

## 8 5.2 The density of GNDs

9 The CTT does not provide a direct approach for calculating the density of GNDs. However,  
10 Nye [11] and Ashby [12] proposed a relation between the density of GNDs and the effective  
11 plastic strain gradient  $\chi^P$ . That is  $\rho_{\text{GND}} = \zeta \chi^P / b$ , where  $\zeta$  is the Nye's factor introduced  
12 by Arsenlis and Parks [66] to characterize the scalar density of GNDs related to the  
13 macroscopic plastic strain gradients. For torsion of FCC polycrystals, the Nye factor is found  
14 to be  $\zeta = 1.93$  [66]. Following Liu *et al.* [2], we assume for wire torsion  $\rho_{\text{GND}} = 2\kappa/b$   
15 when  $r \in [0, r_c]$ , and  $\rho_{\text{GND}} = 0$  when  $r \in [r_c, a]$ . The distributions of GNDs predicted by  
16 CTT are illustrated in Fig. 7(a). One can see that the density of GNDs vanishes in the elastic  
17 zone near the surface of the wire.

18 The distributions of GNDs in the range  $r \in [0, a]$  for three different values of surface  
19 shear strain are shown in Fig. 7(b). One can see that  $\rho_{\text{GND}}$  is mostly flat over a range near

1 the neutral axis, having an obvious transition to a dislocation-free zone outwards the wire  
 2 surface. The dislocation-free zone decreases as the surface shear strain increases. It is worth  
 3 mentioning that an increasing number of the dislocations accumulating in this configuration  
 4 are geometrically necessary. Clearly, the surface depletion of density of GNDs is  
 5 demonstrated.

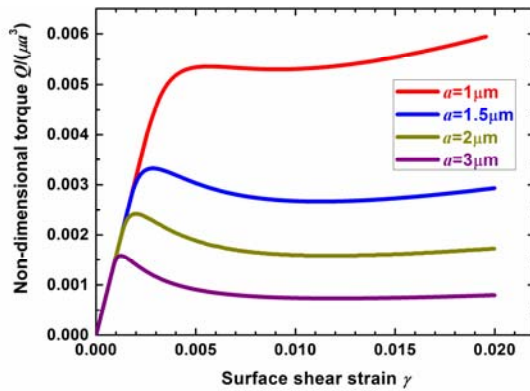


6  
 7 **Fig. 7.** The dislocation density of GNDs as a function of radius  $r$  at the surface strain: (a)  
 8 Prediction given by CCT; (b) Prediction given by CDT.

### 9 5.3 Size effect in the torsion of thin wires by CDT

10 According to CDT (Eq. (45)), the non-dimensional torque  $\hat{Q}$  versus the surface shear  
 11 strain of wires with different diameters is plotted in Fig. 8. One can see that the  
 12 non-dimensional torque increases with decreasing wire radius, which indicates a strong  
 13 influence of wire radius on torsional response. The smaller is the wire radius, the stronger is  
 14 the non-dimensional torque. The theoretical curves show a work hardening around the  
 15 onset of yield due to the dislocation pile up around the neutral axis when  $\gamma > \gamma_{\text{en}}$ . After the  
 16 work-hardening range, there is a strange softening behaviour followed by a further  
 17 work-hardening region. The softening phenomenon is more significant than in the case with  
 18 dissipation, as discussed by Le and Piao [15]. It should be mentioned that, since the  
 19 resistance to the dislocation motion is neglected here, the deformation can be completely  
 20 recoverable when the wire is unloaded. During unloading, the GNDs will move toward the  
 21 free surface upon decreasing the shear stress, and finally slip out from the surface of the

1 wire.



2  
3 **Fig. 8.** Non-dimensional torque versus surface shear strain of wires with various diameters  
4 under elasto-plastic torsion.

## 5 **6. Conclusions**

6 The results of CDT quantitatively elucidate the critical thickness phenomenon appearing in  
7 single-crystalline wires under torsion. The size effect in the initial yielding, the stress  
8 distribution and the distribution of GNDs in the torsion of thin wires, are demonstrated. The  
9 dislocation-free zone near the wire surface and the nearly-zero stress (elastic strain) around  
10 the neutral axis predicted by CDT are in agreement with the results of the CTT. Analysis of  
11 wires in torsion based on CDT shows, as CTT predicts, similar behaviour as in graded-layer  
12 problem, i.e. dislocation sources operate in a GND-free domain near the free surface. This is  
13 the stressed domain, but the GNDs accumulate near the neutral axis. Simulation of  
14 single-crystalline copper wires under torsion based on CDT gives a critical strain-thickness  
15 product around  $0.001 \mu\text{m}$  for different torsion, which is close to the predicted  
16 strain-thickness product of  $0.00128 \mu\text{m}$  by CTT.

17 Strain-thickness products and GND distributions are the key quantities which distinguish  
18 between different theories. The most striking thing about the plots of elastic strain as a  
19 function of position on the cross-sections of the various simulations based on CDT is that  
20 these plots remain very similar. They all show, more or less, a centre region with very little  
21 elastic strain as well as the stress. *A fortiori*, this is where the plastic strain gradient and the

1 density of GNDs are at a maximum. They all show an outer region in which the elastic shear  
2 strain rises in proportion to the radius. Here the plastic strain gradients and the density of  
3 GNDs are small or vanish. This is the region where dislocation sources need to be operated.

4 In summary, we find that:

- 5 • Both CTT and CDT given above are sufficient to give a full quantitative explanation /  
6 understanding of the yield point and early plasticity. GNDs are of course generated and  
7 stored, and pile-ups do occur around the neutral axis, but pile-ups are not the  
8 fundamental explanation of the size effect observed in experiments. A dislocation-free  
9 zone near the wire surface is predicted in both theories.
- 10 • In agreement with bending of foils [44], number (not density) of dislocations determines  
11 what happens, and the size of the specimen determines the stress at which it happens.
- 12 • The size effect at onset of yielding, the distributions of stress and GNDs in the torsion of  
13 thin wires, are simply attributed to the critical thickness effect. A threshold value of  
14 surface shear strain for the dislocation nucleation is indicated in both theories, which is  
15 inversely proportional to the wire radius. If the torsion exceeds the threshold, GNDs  
16 appear to minimize the energy. The size effect in the initial yielding is actually due to the  
17 constraint the geometrical size puts on dislocation curvature.

## 18 Acknowledgments

19 This work is financially supported by the EU's Horizon 2020 research and innovation  
20 programme under the Marie Skłodowska-Curie grant agreement No. 704292. The financial  
21 supports of the National Natural Science Foundation of China (Grant Nos. 11702103,  
22 11472114, 11772138, and 11672251), the Young Elite Scientist Sponsorship Program by CAST  
23 (No. 2016QNRC001), and the Opening Project of Applied Mechanics and Structure Safety Key  
24 Laboratory of Sichuan Province (No. SZDKF-1603) are gratefully acknowledged.

## 25 References

- 26 [1] N.A. Fleck, G.M. Muller, M.F. Ashby, J.W. Hutchinson, Strain gradient plasticity: Theory and  
27 experiment, *Acta Met. Mater.* 42(2) (1994) 475-487.

- 1 [2] D. Liu, Y. He, D.J. Dunstan, B. Zhang, Z. Gan, P. Hu, H. Ding, Toward a further  
2 understanding of size effects in the torsion of thin metal wires: An experimental and  
3 theoretical assessment, *Int. J. Plasticity* 41 (2013) 30-52.
- 4 [3] D.J. Dunstan, B. Ehrler, R. Bossis, S. Joly, K.M.Y. P'NG, A.J. Bushby, Elastic limit and strain  
5 hardening of thin wires in torsion, *Phys. Rev. Lett.* 103(15) (2009) 155501.
- 6 [4] J.W. Hutchinson, Plasticity at the micron scale, *Int. J. Solids. Struct.* 37(1) (2000) 225-238.
- 7 [5] D. Liu, Y. He, X. Tang, H. Ding, P. Hu, Size effects in the torsion of microscale copper wires:  
8 Experiment and analysis, *Scripta Mater.* 66 (2012) 406-409.
- 9 [6] Y. Chen, O. Kraft, M. Walter, Size effects in thin coarse-grained gold microwires under  
10 tensile and torsional loading, *Acta Mater.* 87 (2015) 78-85.
- 11 [7] D. Kiener, W. Grosinger, G. Dehm, R. Pippan, A further step towards an understanding of  
12 size-dependent crystal plasticity: In situ tension experiments of miniaturized single-crystal  
13 copper samples, *Acta Mater.* 56(3) (2008) 580-592.
- 14 [8] M.D. Uchic, D.M. Dimiduk, J.N. Florando, W.D. Nix, Sample dimensions influence strength  
15 and crystal plasticity, *Science* 305(5686) (2004) 986-989.
- 16 [9] D.J. Dunstan, J.U. Galle, B. Ehrler, N.J. Schmitt, T.T. Zhu, X.D. Hou, M. P'Ng K, G. Gannaway,  
17 A.J. Bushby, Micromechanical testing with microstrain resolution, *Rev. Sci. Instrum.* 82(9)  
18 (2011) 093906.
- 19 [10] S. Guo, Y. He, J. Lei, Z. Li, D. Liu, Individual strain gradient effect on torsional strength of  
20 electropolished microscale copper wires, *Scripta Mater.* 130 (2017) 124-127.
- 21 [11] J.F. Nye, Some geometrical relations in dislocated crystals, *Acta Metall.* 1(2) (1953)  
22 153-162.
- 23 [12] M.F. Ashby, The deformation of plastically non-homogeneous materials, *Phil. Mag.*  
24 21(170) (1970) 399-424.
- 25 [13] J.W. Matthews, A.E. Blakeslee, Defects in epitaxial multilayers: I. Misfit dislocations, *J.*  
26 *Cryst. Growth* 27 (1974) 118-125.
- 27 [14] M.H. Kahrobaiyan, S.A. Tajalli, M.R. Movahhedy, J. Akbari, M.T. Ahmadian, Torsion of  
28 strain gradient bars, *Int. J. Eng. Sci.* 49(9) (2011) 856-866.
- 29 [15] K.C. Le, Y. Piao, Distribution of dislocations in twisted bars, *Int. J. Plasticity* 83 (2016)  
30 110-125.
- 31 [16] J. Weertman, Anomalous work hardening, non-redundant screw dislocations in a  
32 circular bar deformed in torsion, and non-redundant edge dislocations in a bent foil, *Acta*  
33 *Mater.* 50(4) (2002) 673-689.
- 34 [17] H. Gao, Y. Huang, W.D. Nix, J.W. Hutchinson, Mechanism-based strain gradient plasticity -  
35 I. Theory, *J. Mech. Phys. Solids* 47(6) (1999) 1239-1263.
- 36 [18] Y. Huang, H. Gao, W.D. Nix, J.W. Hutchinson, Mechanism-based strain gradient plasticity -  
37 II. Analysis, *J. Mech. Phys. Solids* 48(1) (2000) 99-128.
- 38 [19] P. Gudmundson, A unified treatment of strain gradient plasticity, *J. Mech. Phys. Solids*  
39 52(6) (2004) 1379-1406.
- 40 [20] G. Borino, C. Polizzotto, Thermodynamically consistent residual-based gradient plasticity  
41 theory and comparisons, *Modelling Simul. Mater. Sci. Eng.* 15(1) (2007) S23-S35.
- 42 [21] E.C. Aifantis, Strain gradient interpretation of size effects, *Int. J. Fracture* 95(1) (1999)  
43 299-314.
- 44 [22] M.I. Idiart, N.A. Fleck, Size effects in the torsion of thin metal wires, *Modelling Simul.*

- 1 Mater. Sci. Eng. 18 (2010) 015009.
- 2 [23] M. Chircotto, L. Giacomelli, G. Tomassetti, Torsion in strain-gradient plasticity: Energetic  
3 scale effects, Siam. J. Appl. Math. 72(4) (2012) 1169-1191.
- 4 [24] D. Liu, Y. He, L. Shen, J. Lei, S. Guo, K. Peng, Accounting for the recoverable plasticity and  
5 size effect in the cyclic torsion of thin metallic wires using strain gradient plasticity, Mat. Sci.  
6 Eng. A-Struct. 647 (2015) 84-90.
- 7 [25] L. Bardella, A. Panteghini, Modelling the torsion of thin metal wires by distortion  
8 gradient plasticity, J. Mech. Phys. Solids 78 (2015) 467-492.
- 9 [26] V.A. Lubarda, On the recoverable and dissipative parts of higher order stresses in strain  
10 gradient plasticity, Int. J. Plasticity 78 (2016) 26-43.
- 11 [27] E. Bayerschen, A. Prahs, S. Wulfinghoff, M. Ziemann, P.A. Gruber, M. Walter, T. Böhlke,  
12 Modeling contrary size effects of tensile-and torsion-loaded oligocrystalline gold microwires,  
13 J. Mater. Sci. 51 (2016) 7451-7420.
- 14 [28] S.S. Chakravarthy, W.A. Curtin, Stress-gradient plasticity, Proc. Natl. Acad. Sci. USA  
15 108(38) (2011) 15716-15720.
- 16 [29] D. Liu, Y. He, B. Zhang, L. Shen, A continuum theory of stress gradient plasticity based on  
17 the dislocation pile-up model, Acta Mater. 80(0) (2014) 350-364.
- 18 [30] D.J. Dunstan, A.J. Bushby, Theory of deformation in small volumes of material, Proc. Roy.  
19 Soc. Lond. A Mat 460(2050) (2004) 2781-2796.
- 20 [31] A.J. Bushby, D.J. Dunstan, Size effects in yield and plasticity under uniaxial and  
21 non-uniform loading: Experiment and theory, Phil. Mag. 91(7-9) (2011) 1037-1049.
- 22 [32] M. Kaluza, K.C. Le, On torsion of a single crystal rod, Int. J. Plasticity 27(3) (2011)  
23 460-469.
- 24 [33] V.L. Berdichevsky, On a continuum theory of dislocation equilibrium, Int. J. Eng. Sci. 106  
25 (2016) 10-28.
- 26 [34] J. Senger, D. Weygand, O. Kraft, P. Gumbsch, Dislocation microstructure evolution in  
27 cyclically twisted microsamples: a discrete dislocation dynamics simulation, Modelling Simul.  
28 Mater. Sci. Eng. 19(7) (2011) 074004-074004.
- 29 [35] I. Ryu, W. Cai, W.D. Nix, H. Gao, Anisotropic Size-Dependent Plasticity in Face-Centered  
30 Cubic Micropillars Under Torsion, JOM 68(1) (2016) 253-260.
- 31 [36] W. Cai, W. Fong, E. Elsen, C.R. Weinberger, Torsion and bending periodic boundary  
32 conditions for modeling the intrinsic strength of nanowires, J. Mech. Phys. Solids 56(11)  
33 (2008) 3242-3258.
- 34 [37] C.R. Weinberger, W. Cai, Plasticity of metal wires in torsion: Molecular dynamics and  
35 dislocation dynamics simulations, J. Mech. Phys. Solids 58(7) (2010) 1011-1025.
- 36 [38] C.R. Weinberger, W. Cai, Orientation-dependent plasticity in metal nanowires under  
37 torsion: twist boundary formation and eshelby twist, Nano Lett. 10(1) (2010) 139-142.
- 38 [39] H. Zheng, A. Cao, C.R. Weinberger, J.Y. Huang, K. Du, J. Wang, Y. Ma, Y. Xia, S.X. Mao,  
39 Discrete plasticity in sub-10-nm-sized gold crystals, Nat. Commun. 1 (2010) 144.
- 40 [40] M. Stricker, D. Weygand, P. Gumbsch, Irreversibility of dislocation motion under cyclic  
41 loading due to strain gradients, Scripta Mater. 129 (2017) 69-73.
- 42 [41] J.D. Eshelby, Screw dislocations in thin rods, J. Appl. Phys. 24(2) (1953) 176-179.
- 43 [42] J.A. Hurtado, J. Weertman, Non-redundant dislocation density field of a circular bar  
44 deformed in torsion and the stress gradient hardening effect, Phys. Status. Solidi. A 149(1)

- 1 (1995) 173-186.
- 2 [43] D.M. Duan, N.Q. Wu, W.S. Slaughter, S.X. Mao, Length scale effect on mechanical  
3 behavior due to strain gradient plasticity, Mater. Sci. Eng. A-STRUCT 303(1-2) (2001) 241-249.
- 4 [44] C. Motz, D.J. Dunstan, Observation of the critical thickness phenomenon in dislocation  
5 dynamics simulation of microbeam bending, Acta Mater. 60(4) (2012) 1603-1609.
- 6 [45] C.R. Weinberger, The structure and energetics of, and the plasticity caused by, Eshelby  
7 dislocations, Int. J. Plasticity 27(9) (2011) 1391-1408.
- 8 [46] V.L. Berdichevsky, Energy of dislocation networks, Int. J. Eng. Sci. 103 (2016) 35-44.
- 9 [47] M. Ziemann, Y. Chen, O. Kraft, E. Bayerschen, S. Wulffinghoff, C. Kirchlechner, N. Tamura,  
10 T. Böhlke, M. Walter, P.A. Gruber, Deformation patterns in cross-sections of twisted  
11 bamboo-structured Au microwires, Acta Mater. 97 (2015) 216-222.
- 12 [48] D.J. Dunstan, S. Young, R.H. Dixon, Geometrical theory of critical thickness and  
13 relaxation in strained - layer growth, J. Appl. Phys. 70(6) (1991) 3038-3045.
- 14 [49] D.J. Dunstan, Critical Thickness Theory Applied to Micromechanical Testing, Adv. Eng.  
15 Mater. 14(11) (2012) 942-947.
- 16 [50] R. Beanland, Multiplication of misfit dislocations in epitaxial layers, J. Appl. Phys. 72(9)  
17 (1992) 4031-4035.
- 18 [51] E.A. Fitzgerald, Dislocations in strained-layer epitaxy: theory, experiment, and  
19 applications, Mater. Sci. Rep. 7(3) (1991) 87-140.
- 20 [52] D.J. Dunstan, Strain and strain relaxation in semiconductors, J. Mater. Sci-mater. El 8(6)  
21 (1997) 337-375.
- 22 [53] F.C. Frank, J.H. van der Merwe, One-dimensional dislocations. I. Static theory, Proc. Roy.  
23 Soc. Lond. A Mat 198(1053) (1949) 205-216.
- 24 [54] J.W. Matthews, Accommodation of misfit across the interface between single-crystal  
25 films of various face-centred cubic metals, Phil. Mag. 13(126) (1966) 1207-1221.
- 26 [55] D.J. Dunstan, P. Kidd, L.K. Howard, R.H. Dixon, Plastic relaxation of InGaAs grown on  
27 GaAs, Appl. Phys. Lett. 59(26) (1991) 3390-3392.
- 28 [56] D.J. Dunstan, Mathematical model for strain relaxation in multilayer metamorphic  
29 epitaxial structures, Philosophical Magazine A 73(5) (1996) 1323-1332.
- 30 [57] R. Beanland, Dislocation multiplication mechanisms in low - misfit strained epitaxial  
31 layers, J. Appl. Phys. 77(12) (1995) 6217-6222.
- 32 [58] K. Le, P. Sembiring, T. Tran, Continuum dislocation theory accounting for redundant  
33 dislocations and Taylor hardening, Int. J. Eng. Sci. 106 (2016) 155-167.
- 34 [59] V.L. Berdichevsky, On thermodynamics of crystal plasticity, Scripta Mater. 54(5) (2006)  
35 711-716.
- 36 [60] V.L. Berdichevsky, Continuum theory of dislocations revisited, Continuum. Mech. Therm.  
37 18(3-4) (2006) 195-222.
- 38 [61] K.C. Le, C. Günther, Nonlinear continuum dislocation theory revisited, Int. J. Plasticity 53  
39 (2014) 164-178.
- 40 [62] S. Forest, N. Guéninchault, Inspection of free energy functions in gradient crystal  
41 plasticity, Acta Mech. Sinica 29(6) (2013) 763-772.
- 42 [63] I. Groma, G. Gyorgyi, B. Kocsis, Dynamics of coarse grained dislocation densities from an  
43 effective free energy, Phil. Mag. 87(8-9) (2007) 1185-1199.
- 44 [64] J. Senger, D. Weygand, C. Motz, P. Gumbsch, O. Kraft, Evolution of mechanical response

1 and dislocation microstructures in small-scale specimens under slightly different loading  
2 conditions, Phil. Mag. 90(5) (2010) 617-628.

3 [65] D. Zwillinger, Handbook of differential equations, Gulf Professional Publishing1998.

4 [66] A. Arsenlis, D.M. Parks, Crystallographic aspects of geometrically-necessary and  
5 statistically-stored dislocation density, Acta Mater. 47(5) (1999) 1597-1611.

6